

Gone in Seconds: Praxis, Performance, and Peculiarities of Ultrafast Chiral Liquid Chromatography with Superficially Porous Particles

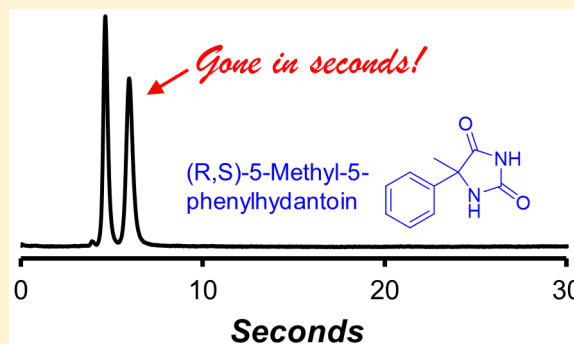
Darshan C. Patel,[†] Zachary S. Breitbach,[†] M. Farooq Wahab,[†] Chandan L. Barhate,[†] and Daniel W. Armstrong^{*,†,‡}

[†]Department of Chemistry and Biochemistry, University of Texas at Arlington, Arlington, Texas 76019, United States

[‡]AZYP LLC, 700 Planetarium Place, Arlington, Texas 76019, United States

S Supporting Information

ABSTRACT: A variety of brush-type chiral stationary phases (CSPs) were developed using superficially porous particles (SPPs). Given their high efficiencies and relatively low back pressures, columns containing these particles were particularly advantageous for ultrafast “chiral” separations in the 4–40 s range. Further, they were used in all mobile phase modes and with high flow rates and pressures to separate over 60 pairs of enantiomers. When operating under these conditions, both instrumentation and column packing must be modified or optimized so as not to limit separation performance and quality. Further, frictional heating results in axial thermal gradients of up to 16 °C and radial temperature gradients up to 8 °C, which can produce interesting secondary effects in enantiomeric separations. It is shown that the kinetic behavior of various CSPs can differ from one another as much as they differ from the well-studied C18 reversed phase media. Three additional interesting aspects of this work are (a) the first kinetic evidence of two different chiral recognition mechanisms, (b) a demonstration of increased efficiencies at higher flow rates for specific separations, and (c) the lowest reduced plate height yet reported for a CSP.



For much of 3 decades, the development and study of chromatographic enantiomeric separations have been dominated by investigations focused on selectivity. This is not surprising given the unique position of chiral separations in chromatography where conventional strategies used for all other molecules are completely ineffective for enantiomers. Hence, the highest impact studies involved conceiving, understanding, and optimizing the use of new and better chiral selectors.^{1–20} Numerous thermodynamic and mechanistic studies as well as evaluations of solvent and additive effects continue even today.^{21–24}

As the field of “chiral separations” has matured, it has focused on other, more typical chromatographic concerns including speed, efficiency, and kinetic effects. While “chiral separations” are ultimately affected by the same parameters as achiral separations, they can have some idiosyncrasies (*vide infra*) as compared to the most extensively studied systems which typically involve reversed phase liquid chromatography on C18 or analogous stationary phases.

The demand for fast and efficient achiral separations provided the impetus for researchers to explore new avenues to increase throughput of chiral screening and analysis. Welch et al. first used multiparallel chiral screening and method development systems that provided method development times of ~1 h.²⁵ Hamman et al. used supercritical fluid chromatography (SFC) at high flow rates, short columns, and a gradient

to obtain a 2.5 min screening method.²⁶ Shortly after, Ai and co-workers developed a bonded sub-1 μm mesoporous silica based cyclodextrin chiral column and published a few 1–6 min enantiomeric separations.²⁷ Concurrently, Gasparrini et al. studied a bonded brush-type (π -complex) phase using sub-2 μm fully porous particles (FPPs) and demonstrated a few normal phase enantiomeric separations in the 15–40 s range.^{28–30}

More recently, superficially porous particles (SPPs) for achiral separations have allowed for column efficiencies comparable to sub-2 μm FPPs while using conventional HPLCs and column hardware.^{31,32} There have been numerous empirical and theoretical comparisons of these approaches when used in a reversed phase (C18) format.^{33–35} SPPs are able to decrease all contributions to band broadening (i.e., longitudinal diffusion, eddy dispersion, and stationary phase mass transfer contributions).³⁵ Initially it was thought that better packing of SPPs was due to their having narrower particle size distributions than FPPs, but it was later shown that better packing homogeneity across the column (i.e., from wall to center of the bed) is largely responsible for the decreased eddy dispersion contribution.^{36,37} Since, SPP columns are

Received: February 20, 2015

Accepted: May 6, 2015

Published: May 6, 2015

generally better packed than FPP columns, they can yield reduced plate heights of 1.3–1.5 for columns packed with conventional achiral stationary phases, whereas FPP based columns typically have reduced plate heights greater than 2.0.³³ Also, the shell thickness of SPPs leads to a shorter trans-particle path length which can decrease mass transfer contributions to band broadening for large molecules with small diffusion coefficients and smaller molecules that have slow adsorption–desorption kinetics.^{31,38,39} This is particularly important at higher flow rates.

The possible benefits of SPPs in other important but more specialized areas of LC are less explored. Chankvetadze compared a polysaccharide based chiral selector coated on FPPs and SPPs in both nano-LC and HPLC.^{40,41} In the latter, an obvious decrease in enantiomeric selectivity was noted for the SPP based material. Gritti and Guiochon's theoretical treatment of the same polysaccharide based chiral selector indicated that a 10% gain in resolution (R_s) could be possible due to the decreased plate heights afforded by the SPPs.⁴² However, this estimated value was based on an assumption that the SPP based polysaccharide column would have a similar enantiomeric selectivity value as the analogous FPP based column which, as noted, has not been obtainable to date. Most recently, Spudeit et al. presented the first successful and practical SPP CSP.³⁹ This work showed that brush-type chiral selectors (i.e., isopropylcarbamated cyclofructan 6) have a higher chiral selector load (per surface area). This plus the observed increase in column efficiency for the SPP based CSP resulted in improved enantiomeric separations, while maintaining the same enantiomeric selectivity as FPP based CSPs.³⁹ Further, the SPP CSP maintained this performance with 50–75% lower retentions. When comparing constant retention modes, the R_s values obtained using the SPP column were far greater than the FPP columns. It was also noted that as flow rates increased (e.g., to 3 mL/min), the resolution per analysis time greatly improved for the SPP column (by 18–67%) meaning that high-throughput screening would benefit from such columns.³⁹

In this work, a broad range of analyte types and polarities including pharmaceuticals, catalysts, peptides, amino acids, primary amines, and biaryls among others were baseline separated on a variety of SPP brush type CSPs that are very effective for ultrafast chiral separations (~4–40 s range). It is demonstrated that they can be performed in any mobile phase conditions or mode, i.e., reversed phase, normal phase, polar organic, and HILIC. Finally, the practice of ultrafast chiral LC often produces interesting and unusual consequences that must be recognized, dealt with, and/or properly understood for optimal performance.

■ EXPERIMENTAL SECTION

Materials. All HPLC solvents and reagents for reactions were purchased from Sigma-Aldrich (St. Louis, MO). Cyclofructan-6 (CF6) and cyclofructan-7 (CF7) derivatized with isopropyl carbamate and dimethylphenyl carbamate groups, respectively, were synthesized by AZYP LLC (Arlington, TX). The 2.7 μm superficially porous silica particles with a surface area of 120 m^2/g and pore size of 120 Å were provided by Agilent Technologies (Wilmington, DE). The core is 1.7 μm in diameter and the surrounding shell thickness is 0.5 μm . The fully porous 2.1 and 3 μm silica particles were purchased from Daiso (Tokyo, Japan) and Glantreo (Cork, Ireland), respectively. The 2.1 μm fully porous particles have a surface

area of 479 m^2/g and pore size of 91 Å, whereas the 3 μm fully porous particles have a surface area of 300 m^2/g and pore size of 100 Å. Tröger's bases were obtained as indicated in the literature.⁴³ All solvent mixtures are given in (v/v).

Synthesis of Stationary Phases. All reactions were carried out in anhydrous solvents under a dry argon atmosphere. The synthetic procedures for the six stationary phases employed in this work have already been published.^{10,13,16,18,44} The first chiral stationary phases explored were cyclofructan based as they have recently proven to be unique chiral selectors.^{18,45–50} The cyclofructan-6 derivatized isopropyl carbamate (CF6-P) and cyclofructan-7 dimethylphenyl carbamate (CF7-DMP) were bonded to silica particles under anhydrous conditions as described previously.¹⁸ The 2-hydroxypropyl- β -cyclodextrin bonded silica (CD-HP) was synthesized via a proprietary bonding procedure.^{10,44} Macrocylic antibiotics vancomycin, teicoplanin, and teicoplanin aglycone were covalently attached to silica surface as described by Armstrong et al.^{13,16} Each of the above chiral selectors were bonded to 2.7 μm SPPs. The 2.1 and 3 μm fully porous particles were functionalized with CF6-P. The CHN analyses of the phases and chiral selector coverage per surface are provided in Table S2 in the Supporting Information.

Each stationary phase was slurry packed with a pneumatically driven Haskel pump (DSTV-122) into 10 cm \times 0.46 cm i.d., 5 cm \times 0.46 cm i.d., and 3 cm \times 0.46 cm i.d. stainless steel columns (IDEX Health and Science, Oak Harbor, WA). See the Supporting Information for the packing method (Figure S1). Commercial LARIHC CF6-P, LARIHC CF7-DMP, Chirobiotic V, Chirobiotic T, Chirobiotic TAG, and Cyclobond I 2000 HP-RSP columns (fully porous 5 μm particles, 25 cm \times 0.46 cm i.d.) which were used for comparative purposes were provided by AZYP LLC, Astec, and Supelco/Sigma-Aldrich.

Instrumentation. All ultrafast separations were performed on an Agilent 1290 Infinity series UHPLC system (Agilent Technologies, Santa Clara, CA) equipped with a quaternary pump, an auto-sampler, and a diode array detector. Routine separations were performed on an Agilent 1260 HPLC equipped with a quaternary pump, an auto-sampler, and a diode array detector. An inlet filter was installed between the pump outlet and the auto-sampler injection valve to prevent clogging of 75 μm tubings. For fast separations, the data collection rate was set at 160 Hz with a response time of 0.016 s, unless otherwise stated. The thermostated column compartment and the column switching 6-port valve were bypassed to minimize the length of connection tubings. The instrument was further optimized to reduce extra-column effects by using an ultralow dispersion kit from Agilent (P/N 5067-5189). The kit consists of an ultralow dispersion needle and needle seat, two 75 μm i.d. stainless steel connection tubings, and a detector flow cell with a volume standard deviation $V(\sigma)$ of 0.6 μL . Alternatively, 75 μm i.d. polyether ether ketone (PEEK) nanoViper connection tubings (Thermo Fisher Scientific, MA) were also employed. The instrument was controlled by OpenLAB CDS ChemStation software (Rev. C.01.06 [61], Agilent Technologies 2001–2014) in Microsoft Windows 8.1 (see the Supporting Information for the calculation of peak parameters). The reported percentages of mobile phases (m.p.) are listed as volume/volume (v/v).

Axial Temperature Gradient in Mobile Viscous Frictional Heating. The effect of viscous frictional heating of the mobile phases in the SPP columns was studied by wrapping the column in an insulating sheet (at room temperature) and

inserting a Mastech thermocouple MS8222H (Pittsburgh, PA) inside the column outlet with the help of a screw cap. The flow rate was varied and the resulting temperature was monitored after 10 min of equilibration.

DISCUSSION

Figure 1A provides comparisons of different particle size fully porous particles (FPPs) and superficially porous particles

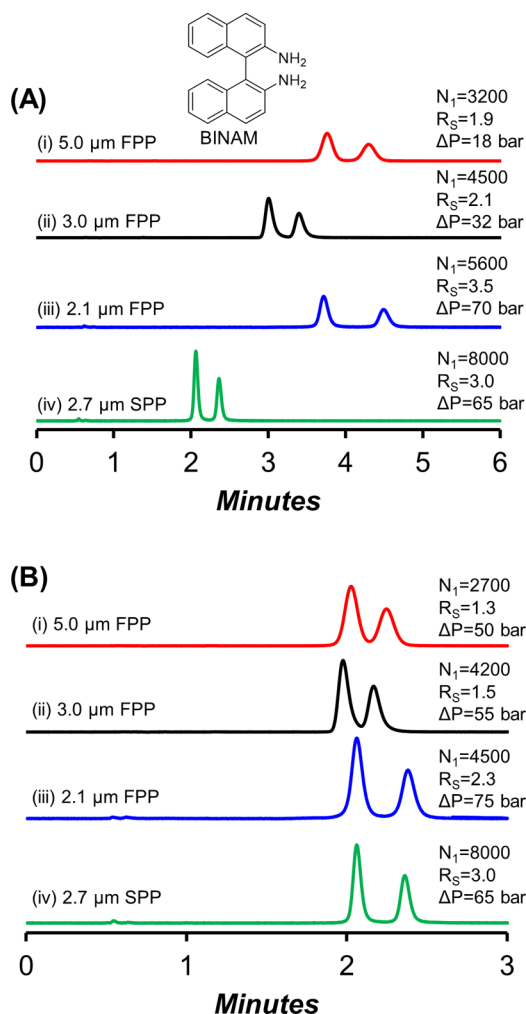


Figure 1. Enantiomeric separations of BINAM on CF6-P bonded to SPPs and FPPs at 1.0 mL/min, $T_{\text{col}} = 25^\circ\text{C}$. All columns were 5 cm \times 0.46 cm in dimensions. (A) Constant MP mode, MP = 92:8 heptane-ethanol. (B) Constant retention mode, MP = (i) 82:18 heptane-ethanol, (ii) 85:15 heptane-ethanol, (iii) 82:18 heptane-ethanol, and (iv) 92:8 heptane-ethanol.

(SPPs) which have the same bonded chiral selector (via the same chemistry) and with the same mobile phase. These chromatograms were generated using conventional HPLCs with conventional conditions and column sizes (i.e., 1.0 mL/min flow rate and 5 cm \times 0.46 cm i.d. columns). Clearly using the same mobile phase, the SPP-based CSP provided both the greatest efficiency and shortest analysis time as compared to all FPPs, including the 2.1 μm particles (Figure 1A). However, according to Gritti and Guiochon, a better comparison of such columns is realized when resolutions (R_s) are compared at constant retention (Figure 1B).⁴² They also indicated that a SPP's core to particle diameter ratio (ρ) can be related to its

gain in resolution. Specifically ρ values between 0.5 and 0.95 at constant retention factor (k) can slightly improve the resolution. Interestingly, recent work on a brush-type CSP showed a resolution increase of 20%.³⁹ In Figure 1B, the increase in resolution of the SPP-CSP over both 3 and 2.1 μm FPPs is $\sim 30\%$, which is quite impressive. The SPP-CSP used here had a ρ value of 0.63 (see Experimental Section), which is within the optimal range (*vide supra*).⁴² A direct comparison of the efficiencies, reduced plate heights, and tailing factors of current commercial columns (5 μm particles) and the analogous CSPs on 2.7 μm SPPs is given in Table 1. The 3–

Table 1. Comparison of Theoretical Plates/Meter (N/m), Reduced Plate Height (h), and USP Tailing Factor Using a Standard Achiral Probe 1,3-Dinitrobenzene with 70:30 Heptane–Ethanol at Reduced Velocity of 4.5 (1 mL/min for 2.7 μm SPP, 0.6 mL/min for 5 μm FPP)

stationary phase	N/m^a	h	tailing factor ^b
<i>Stationary Phases Bonded to 2.7 μm SPPs</i>			
CF6-P ^c	172 000	2.2	1.1
CF7-DMP ^d	221 000	1.6	1.2
teicoplanin ^d	165 000	2.3	1.0
teicoplanin aglycone ^c	133 000	2.8	1.3
vancomycin ^c	173 000	2.1	0.9
hydroxypropyl- β -cyclodextrin ^d	181 000	2.0	1.3

Commercial Columns Packed with 5.0 μm FPPs (25 cm \times 0.46 cm)

LARIHC CF6-P	70 000	2.9	1.1
LARIHC CF7-DMP	59 000	3.4	1.2
Chirobiotic-T	54 000	3.7	0.9
Chirobiotic-TAG	50 000	4.0	1.1
Chirobiotic-V	57 000	3.5	0.9
Cyclobond I 2000 HP-RSP	37 000	5.4	1.1

^a N/m calculated by half height method. ^bUSP tailing factor $T = W_{0.05}/2f$, where $W_{0.05}$ = peak width at 5% peak height and f = distance from the leading edge of the peak to the peak maximum at 5% peak height. ^cDimensions of these columns were 10 cm \times 0.46 cm. ^dDimensions of these columns were 5 cm \times 0.46 cm.

4-fold increase in efficiencies is impressive but not totally unexpected given the smaller SPP particle diameter. However, the reduced plate heights of the SPPs also are up to 2 times smaller and with comparable or better peak symmetries. The reduced plate height (h) of 1.6 for the CF7-DMP SPP is the smallest reported for any CSP on any particle to date. Given these results, it is clear that SPP based CSPs should be particularly advantageous for ultrafast chiral separations.

In the literature, the current accepted time limit for being labeled as an ultrafast chromatographic separation seems to be ~ 1 min.^{51,52} This is probably a reasonable choice since typical HPLC autoinjectors cycle at ~ 1 injection per min (or down to 0.5 min for UHPLC). Hence in ultrafast LC, the chromatographic separations can be completed more quickly than new samples can be injected (by conventional injection devices). Figure 2 and Table 2 show over 60 such baseline enantiomeric separations. The table covers a wide structural variety of enantiomers. Most separations are <40 s and almost a quarter of those are on the order of 10 or fewer seconds. Furthermore, these are accomplished in all mobile phase modes, i.e., normal phase, reversed phase, and polar organic modes and on a variety of bonded CSPs. Theoretically, we could screen ~ 90 to 360 chiral analytes per hour which could use less solvent than any

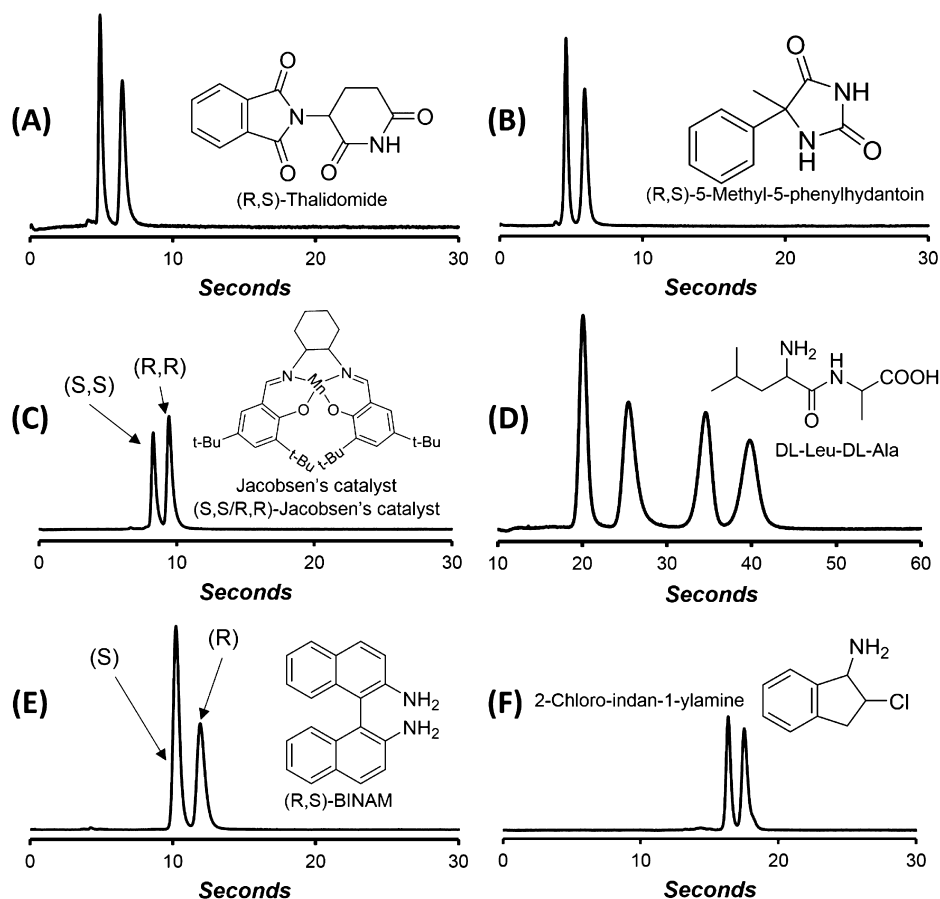


Figure 2. Representative ultrafast enantiomeric separations on each of 6 chiral stationary phases: (A) vancomycin SPP (3 cm \times 0.46 cm), MP = methanol, 4.95 mL/min, $T_{\text{col}} = 60^\circ\text{C}$; (B) teicoplanin aglycone SPP (3 cm \times 0.46 cm), MP = methanol, 4.70 mL/min, $T_{\text{col}} = 60^\circ\text{C}$; (C) hydroxylpropyl- β -cyclodextrin SPP (5 cm \times 0.46 cm), MP = 97:3:0.3:0.2 acetonitrile–methanol–TFA–TEA, 4.75 mL/min, $T_{\text{col}} = 60^\circ\text{C}$; (D) teicoplanin SPP (3 cm \times 0.46 cm), MP = 40:60 water–methanol, 3.00 mL/min, $T_{\text{col}} = 22^\circ\text{C}$; (E) CF7-DMP SPP (3 cm \times 0.46 cm), MP = 90:10 heptane–ethanol, 4.80 mL/min, $T_{\text{col}} = 22^\circ\text{C}$; (F) CF6-P SPP (10 cm \times 0.46 cm), MP = 70:30:0.3:0.2 acetonitrile–methanol–TFA–TEA, 4.50 mL/min, $T_{\text{col}} = 22^\circ\text{C}$.

other current method. However, this is restricted to ~ 60 to, at most, 120 samples/hour because of instrumental autoinjector limitations. Certainly, this is not the first nor the only example of chromatographic potential being limited by instrumental deficiencies.^{51,53} Indeed, as discussed in the following paragraphs, the separations shown in Figure 2 and listed in Table 2 cannot be achieved under standard HPLC conditions used for Figure 1.

Effect of Packing on Columns Used for Ultrafast Chiral LC. Accomplishing ultrafast separations in HPLC generally requires higher flow rates, higher pressures, and shorter columns. Consequently, both the column packing quality and permeability are important. Commercial packing procedures are usually trade secrets. When packing identical columns with different slurry solvents, it was found that the use of a “well dispersed” slurry produced columns of $>2.3\times$ higher efficiencies and slightly different permeability according to Darcy’s law (see Figures S1 and S2 and the associated text followed in the Supporting Information).

Detector Sampling Rates and Response Times. The detector sampling rate (a.k.a. sampling frequency, data acquisition frequency or rate, etc.) and the detector response time become increasingly important for rapidly eluting analytes and highly efficient separations as demonstrated with SPPs. Under certain circumstances, peak shapes, peak width, and

baseline noise can vary considerably as a result of detector settings. There is some debate as to the exact cause and nature of these effects.⁵⁴ We will address this debate in a subsequent communication but will only present the empirical results, as it impacts enantiomeric separations herein. Figure 3 shows the effect of detector sampling rate and response time (for an Agilent 1290 UHPLC) on the efficiency (N), resolution (R_s), and baseline noise for six ultrafast enantiomeric separations performed under otherwise identical conditions. Note that with Agilent ChemStation software, the detector sampling rate and response times are coupled and the operator cannot independently change or “unpair” these two parameters. The observed effects are the combined result of these two parameters. At the lowest sampling rate and longest response time (bottom curve, Figure 3), the separation is not discernible, the apparent efficiency and resolution is poor, but there is little baseline noise. The separation parameters improve tremendously as the sampling rate increases and the coupled time constant decreases up to about the 80 Hz curve. Concurrently the noise level increases (see 80 \times zoom in Figure 3). The default setting on this instrument is 2.5 Hz. It should be noted that with other instruments (Dionex and Shimadzu, for example) the operator can independently set these detector settings which could relate in an array of unwanted or suboptimal combinations. It is apparent that to maintain high

Table 2. Chromatographic Data for Optimized Ultrafast Chiral Separations on Six Different Chiral Stationary Phases (CSP) Bonded to 2.7 μm Superficially Porous Particles^a

#	Analyte	Structure	CSP ^b	mobile phase; flow rate	t _{R1} sec	t _{R2} sec	R _s ¹
1	Alanine		T	25:75 water:MeOH; 3.1 mL/min	12	18	3.2
			TAG	70:30 water:MeOH; 2.5 mL/min	10	13	2.2
2	Phenylalanine		T	25:75 water:MeOH; 2.5 mL/min	15	21	2.2
			TAG	40:60 water:MeOH; 2.5 mL/min	15	22	2.1
3	4-Chlorophenylalanine		TAG	40:60 water:MeOH; 2.5 mL/min	17	26	1.9
4	Threonine		T	10:90 water:MeOH; 2.9 mL/min	13	17	1.6
			TAG	25:75 water:MeOH; 2.5 mL/min	11	15	2.6
5	Methionine		T	90:10 water:MeOH; 3.7 mL/min	8	9	1.5
			TAG	90:10 water:MeOH; 3.3 mL/min	9	12	2.3
6	Valine		T	25:75 water:MeOH; 2.5 mL/min	10	15	2.6
			TAG	90:10 water:MeOH; 2.2 mL/min	11	14	1.6
7	Norvaline		T	80:20 water:MeOH; 3.0 mL/min	8	10	1.5
			TAG	80:20 water:MeOH; 3.0 mL/min	8	13	2.1
8	Leucine		T	10:90 water:MeOH; 2.9 mL/min	13	23	3.2
			TAG	90:10 water:EtOH; 3.0 mL/min	9	12	1.9
9	Isoleucine		T	60:40 water:MeOH; 2.5 mL/min	11	14	1.7
			TAG	90:10 water:MeOH; 2.5 mL/min	11	14	1.6
10	Norleucine		T	60:40 water:MeOH; 2.5 mL/min	11	15	2.3
			TAG	60:40 water:MeOH; 2.5 mL/min	13	17	1.7
11	Tyrosine		T	25:75 water:MeOH; 2.5 mL/min	14	18	2.0
			TAG	60:40 water:MeOH; 2.5 mL/min	13	18	1.7
12	m-Tyrosine		T	90:10 water:EtOH; 3.7 mL/min	9	12	1.9
			TAG	99:1 water:MeOH; 3.7 mL/min	10	31	2.5
13	o-Tyrosine		TAG	15:85 water:MeOH; 3.0 mL/min	16	23	1.6
14	Homophenylalanine		T	90:10 water:MeOH; 3.5 mL/min	12	18	2.7
			TAG	60:40 water:MeOH; 2.2 mL/min	17	39	3.1
15	Homoserine		TAG	50:50 water:MeOH; 2.5 mL/min	10	13	1.5
16	Proline		T	90:10 water:MeOH; 3.7 mL/min	8	13	3.6
			TAG	90:10 water:MeOH; 3.0 mL/min	10	17	2.5
17	2-Phenylglycine		T	90:10 water:MeOH; 3.5 mL/min	9	15	3.3
			TAG	30:70 water:MeOH; 2.7 mL/min	7	14	3.7
18	6-methyl-Tryptophan		T	25:75 water:MeOH; 2.5 mL/min	17	23	1.9
19	3-(1-Naphthyl)alanine		T	25:75 water:MeOH; 2.5 mL/min	19	26	1.8

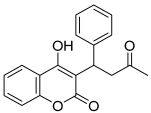
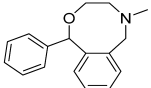
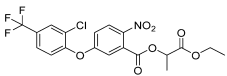
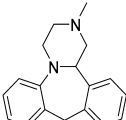
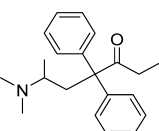
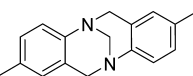
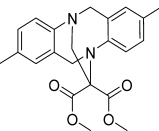
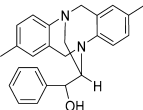
Table 2. continued

#	Analyte	Structure	CSP ^b	mobile phase; flow rate	t _{R1} sec	t _{R2} sec	R _S ¹
20	3,5-DNB-Tryptophan methyl ester		CF7-DMP	70:30:0.1 heptane:EtOH:TFA, 3.0 mL/min	38	44	1.9
21	BINAM		CF7-DMP	90:10 heptane:EtOH, 4.8 mL/min	10	12	1.9
22	NOBIN		CF7-DMP	98:2 heptane:EtOH, 4.5 mL/min	17	22	2.5
23	Vanol		CF6-P ^c	98.5:1.5 heptane:EtOH, 3.5 mL/min	29	33	1.7
24	(1R,2S/1S,2R) 2-Amino-1,2-diphenylethanol		CF6-P ^d	70:30:0.3:0.2 ACN:MeOH:TFA:TEA, 4.0 mL/min	18	20	1.8
25	(1S,2S/1R,2R) 2-Amino-1-(4-nitrophenyl)-1,3-propanediol		CF6-P ^d	80:20:0.3:0.2 ACN:MeOH:TFA:TEA, 4.0 mL/min	28	30	1.6
26	2,4-Dichloro-α-phenethylamine		CF6-P ^c	90:10:0.3:0.2 ACN:MeOH:TFA:TEA, 5.0 mL/min	12	14	1.8
27	2-Chloro-indan-1-ylamine hydrochloride		CF6-P ^c	90:10:0.3:0.2 ACN:MeOH:TFA:TEA, 4.5 mL/min	12	14	1.6
28	1(1-naphthyl)ethylamine		CF6-P ^d	80:20:0.3:0.2 ACN:MeOH:TFA:TEA, 4.5 mL/min	23	25	1.9
29	(1S,2S/1R,2R) trans-1-Amino-2-indanol		CF6-P ^c	92:8:0.3:0.2 ACN:MeOH:TFA:TEA, 5.0 mL/min	20	26	1.8
30	α-Ethylbenzylamine		CF6-P ^d	80:20:0.3:0.2 ACN:MeOH:TFA:TEA, 4.0 mL/min	30	32	1.6
31	1-biphenyl-4-yl-ethylamine		CF6-P ^d	80:20:0.3:0.2 ACN:MeOH:TFA:TEA, 3.0 mL/min	38	40	1.5
32	Norphenylephrine hydrochloride		CF6-P ^d	75:25:0.3:0.2 ACN:MeOH:TFA:TEA, 3.7 mL/min	36	39	1.5
33	Normetanephrine hydrochloride		CF6-P ^d	75:25:0.3:0.2 ACN:MeOH:TFA:TEA, 3.6 mL/min	34	37	1.5
34	(1S,2S/1R,2R) 2-Amino-1-(4-nitrophenyl)-1,3-propanediol		CF6-P ^d	80:20:0.3:0.2 ACN:MeOH:TFA:TEA, 4.0 mL/min	28	30	1.6
35	Tryptophanol		CF6-P ^d	80:20:0.3:0.2 ACN:MeOH:TFA:TEA, 4.0 mL/min	27	30	1.5
36	DL-Ala-DL-Ala ^c		T	40:60 water:MeOH, 3.3 mL/min	18	26	2.5
37	DL-Leu-DL-Ala ^c		T	40:60 water:MeOH, 3.0 mL/min	20	25	2.4

Table 2. continued

#	Analyte	Structure	CSP ^b	mobile phase; flow rate	t _{R1} sec	t _{R2} sec	R _s ¹
38	DL-Leu-DL-Leu ^c		T	40:60 water:MeOH, 3.3 mL/min	18	27	2.5
39	Gly-DL-Ala		T	40:60 water:MeOH, 3.3 mL/min	20	49	5.8
40	Gly-DL-Met		T	40:60 water:MeOH, 3.3 mL/min	19	55	6.4
41	Gly-DL-Phe		T	40:60 water:MeOH, 3.3 mL/min	21	49	5.0
42	5-Methyl-5-phenylhydantoin		T ^f	MeOH, 4.7 mL/min	5	5	1.5
			TAG ^f	MeOH, 4.7 mL/min	5	6	2.4
			V	90:10 1% TEAA pH 7:ACN, 3.0 mL/min	15	17	1.7
43	Jacobsen's catalyst		CD-HP ^{c,f}	97:3:0.3:0.2 ACN:MeOH:TFA:TEA, 4.75 mL/min	8	9	1.8
44	3-Phenylphthalide		T	50:50 1% TEAA pH 4.1:MeOH, 2.6 mL/min	15	20	1.9
45	Propanolol		T	70:30:0.3:0.2 ACN:MeOH:AA:TEA, 4.0 mL/min	29	33	1.6
46	Sotalol		T ^c	60:40:0.3:0.2 ACN:MeOH:AA:TEA, 4.0 mL/min	20	22	1.5
47	Alprenolol		T ^c	65:35:0.3:0.2 ACN:MeOH:AA:TEA, 4.0 mL/min	21	24	1.5
48	Mandelic Acid		T	50:50 1% TEAA pH 4.1:MeOH, 2.4 mL/min	6	8	1.9
49	Thalidomide		V ^f	MeOH, 4.95 mL/min	5	6	2.7
50	Nicardipine		V	100:0.1 mM MeOH:NH ₄ TFA, 1.0 mL/min	29	34	1.7
51	Proglumide		V	80:20 1% TEAA pH 4.1:ACN, 4.0 mL/min	15	18	1.5
52	Coumachlor		V	80:20 1% TEAA pH 4.1:ACN, 4.5 mL/min	30	38	1.7

Table 2. continued

#	Analyte	Structure	CSP ^b	mobile phase; flow rate	t _{R1} sec	t _{R2} sec	R _S ¹
53	Warfarin		V	85:15 1% TEAA pH 4.1:ACN, 4.0 mL/min	29	36	1.5
54	Nefopam		CD-HP ^c	65:35 20 mM NH ₄ OAc:ACN, 2.5 mL/min	35	40	2.1
55	Lactofen		CF7-DMP ^c	98:2:0.1 heptane:IPA:TFA, 2.0 mL/min	31	34	1.8
56	Mianserin		V	100:0.15:0.05 MeOH:AA:TEA, 4.0 mL/min	15	19	1.7
57	Methadone		CD-HP ^c	78:22 0.1% AA in water:ACN, 3.7 mL/min	26	30	1.6
58	Tröger's base		CF7-DMP ^c	70:30 heptane:EtOH, 2.5 mL/min	18	20	1.8
59	Ethano-bridged Tröger's base 1		CD-HP ^c	57:43 20 mM NH ₄ OAc pH 4.1:EtOH, 1.3 mL/min	31	38	1.6
60	Ethano-bridged Tröger's base 2		CD-HP ^c	55:45 20 mM NH ₄ OAc pH 4.1:ACN, 2.0 mL/min	24	28	1.6

^aAll separations were performed on an Agilent 1290 UHPLC instrument optimized for low extra column volume. See Supporting Information for more information on R_S. Column dimensions for all separations were 3 cm × 0.46 cm and column temperature was ambient (~22 °C) unless otherwise stated. ^bT = teicoplanin, TAG = teicoplanin aglycone, CF7-DMP = Cyclofructan-7 dimethylphenyl carbamate, CF6-P = Cyclofructan-6 isopropyl carbamate, V = vancomycin, CD-HP = hydroxypropyl-β-cyclodextrin. ^cDimensions of column = 5 cm × 0.46 cm. ^dDimensions of column = 10 cm × 0.46 cm. ^eData for the 1st eluted enantiomers. ^fT_{col} = 60 °C.

efficiency and good resolution when doing ultrafast separations that detector coupled sampling rates should be ≥40 Hz and response time ≤0.13 s (Figure 3). For enantiomeric separations <10 s, even higher rates and lower times are needed. If one is simply screening samples and concentration is not a factor, the choice of detector settings are straightforward (e.g., 80 or 160 Hz). However, if one is examining either very low amounts of an analyte or enantiomeric purities, the higher baseline noise (top curve in Figure 3) can obscure low level enantiomeric impurities (e.g., <1% and especially <0.1%) and decrease the accuracy and precision of the measurement.

Extra Column Band Broadening Effects on Ultrafast Separations. It is well established that extra column band broadening is a concern when using short and/or narrow-bore columns that often are packed with smaller diameter particles, as in UHPLC.⁵⁵ In this regard, chiral separations are no different, especially when doing ultrafast separations where it is essential to maintain high efficiencies. Figure 4 illustrates this assessment. A “stock” UHPLC was tested (top chromatogram, Figure 4) and then the “extra column parts” of the instrument were replaced with smaller volume versions. Using the variance

(σ²) calculated from second moment analysis, intrinsic column efficiencies were calculated in each case, reflecting the true column efficiency of 4750 plates for a 20 s separation (see the Supporting Information). The σ²_{ratio} was also calculated using the relationship σ²_{ratio} = σ²_{system}/σ²_{column+system}. As can be seen, a complete system optimization produced a decrease in the extra column variance ratio from 26% to 3% and this resulted in an ultrafast enantiomeric separation that went from ~71 000 plates/m and a resolution of 1.4 to ~94 000 plates/m and a resolution of 1.7.

Kinetic and Thermal (Frictional) Considerations. Both the general topic of column efficiency and the more specific issue of frictional heating have been considered for columns containing small particles (e.g., <2 μm diameter) and for narrow bore columns.⁵⁶ Most of these studies focused on reversed phase C18 based column formats.^{57–61} There are few kinetic studies on small particle and SPP chiral stationary phases (CSPs) and none on the effect of frictional heating on these CSPs.^{40–42} As stated previously, CSPs are subject to the same thermodynamic and kinetic constraints as other column types. However, the manifestation of these kinetic terms can

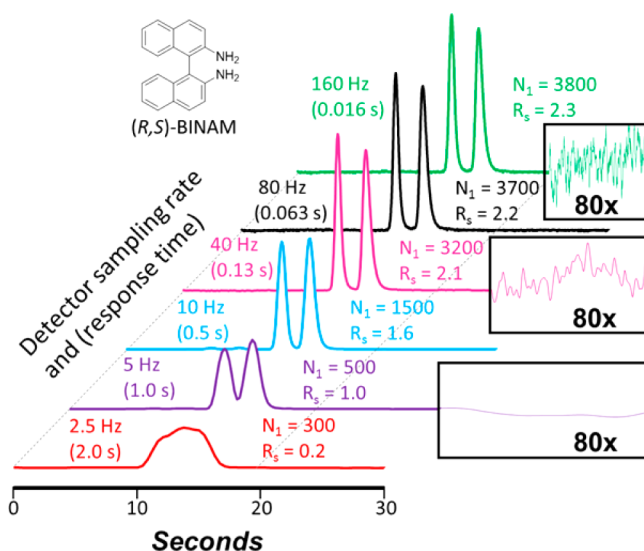


Figure 3. Effect of detector sampling rate and response time on efficiency (N) and resolution (R_s) in ultrafast chromatographic separations. BINAM analyzed on CF7-DMP SPP (3 cm \times 0.46 cm), MP = 90:10 heptane–ethanol, 4.0 mL/min, T_{col} = 22 $^{\circ}$ C; 1 Hz = 1 s $^{-1}$.

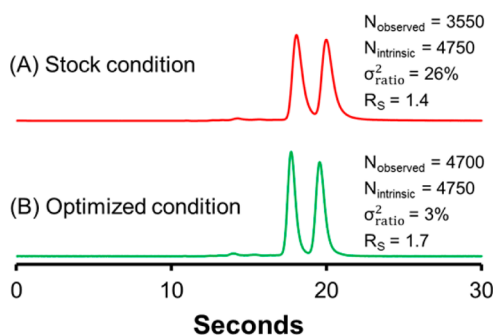


Figure 4. Optimization of Agilent 1290 UHPLC for ultrafast separations by replacing stock parts with low extra column volume alternatives. Tröger's base analyzed on CF7-DMP SPP (5 cm \times 0.46 cm), MP = 70:30 heptane–ethanol, 2.5 mL/min, T_{col} = 22 $^{\circ}$ C. Percent extra column contribution is expressed as $\sigma_{ratio}^2 = \sigma_{system}^2 / \sigma_{column+system}^2$ (see the Supporting Information for moment analysis). (A) Stock condition: stock injection needle and needle seat, 170 μ m i.d. connection tubing (22 cm total) with IDEX 10-32 finger tight fittings, and a 1.0 μ L detector flow cell. (B) Optimized conditions: ultralow dispersion needle and needle seat, 75 μ m i.d. nanoViper connection tubing (22 cm total), 0.6 μ L detector flow cell.

differ as much from one CSP to another as they do from conventional C18 or silica gel stationary phases. Likewise, the effect of frictional heating and column temperature gradients has been evaluated and discussed for C18 reversed phase columns.^{57,59,61} For SPP-based CSPs, differences as well as any peculiarities can be revealed by any of the related kinetic plots (van Deemter, reduced van Deemter, or Knox).⁵⁶ For the purpose of this discussion, we will use the standard Giddings' coupled van Deemter equation of:

$$H = \frac{B}{u} + C_s u + C_{SM} + \left(\frac{1}{A} + \frac{1}{C_M} \right)^{-1} \quad (1)$$

where H is the height equivalent to a theoretical plate, A is the eddy dispersion term, B is the longitudinal diffusion term, C_s is stationary phase mass transfer, C_{SM} is mass transfer in the

stagnant mobile phase (sometime treated as "short range" eddy dispersion), C_M is the moving mobile phase mass transfer term, and u is the linear velocity (m/s) of the mobile phase.⁶²

Figure 5 shows four unique sets of van Deemter plots done in the (A) polar organic mode, (B) normal phase mode, and (C and D) in the reversed phase mode under two different temperature conditions. Each set of curves contains one pair of enantiomers and at least one achiral test molecule. The experimental conditions are given in the legend. The solvent temperature at the column outlet was measured at different linear velocities and mobile phase modes (see the Experimental Section and Supporting Information).

The "polar organic" plots in Figure 5A indicate what some would consider to be a normal "well behaved" system. The achiral void volume marker (1,3-dinitrobenzene) has the lowest H at all linear velocities above ~ 0.5 mm/s and the flattest rise at higher velocities. The least retained (first eluted) enantiomer and a retained achiral analyte (nicotinamide) had almost identical efficiencies at all linear velocities and similar, slightly greater slopes at higher linear velocities. The most retained enantiomer is generally thought to have the greatest resistance to stationary phase mass transfer as it is subject to a greater number of associative stereochemical interactions and often reorientation of the enantiomer.^{22,63} This appears to be so as the H_{min} is at a slightly lower linear velocity for the second enantiomer compared to the first enantiomer and the achiral probe, indicating an increase in the C_s term.

Figure 5B shows the analogous plots for the enantiomers of Tröger's base as well as retained and unretained achiral probe molecules in the normal phase mode. The relative kinetic behaviors of these molecules are quite different than those in Figure 5A. The plots of the enantiomers are almost identical at all linear velocities. However, this behavior is believed to be related to two different things, one of which relates to the stereochemical recognition mechanism while the other is related to general column properties. The similar kinetic behaviors of the two enantiomers indicate that chiral recognition is likely due to the presence of repulsive (steric) interactions rather than multiple associative interactions with one of the enantiomers. For example, the minimum 3-point of interaction needed for chiral recognition could come from one associative interaction plus 2 steric interactions with one of the enantiomers. The only requirement of this model is that the total energy of association be greater than that of the combined steric repulsive interactions. Such systems have been proposed previously, but this is the first time kinetic data has been used to support such a scenario.^{22,63}

Also important is the relative behavior of the retained and unretained achiral analytes in Figure 5B which is opposite to that in Figure 5A. The unretained void volume marker (1,3,5-tri-*tert*-butylbenzene) has worst efficiency at all linear velocities but a flatter rise than the enantiomers at higher linear velocities. The retained achiral molecule (1,3-dinitrobenzene) exhibited the highest efficiency at all linear velocities and had the flattest rise at higher linear velocities. This type of behavior has been reported previously in a few instances for well packed, high efficiency columns.^{55,64} The van Deemter curves in Figure 5B were produced using a standard HPLC with a conventional injector, tubings, column compartment, and detector flow cell. When the extra column effects were minimized (Figure 4), the observed efficiencies of the 1,3,5-tri-*tert*-butylbenzene and 1,3-dinitrobenzene were nearly identical. This clearly illustrates the pronounced effects of extra column band broadening on

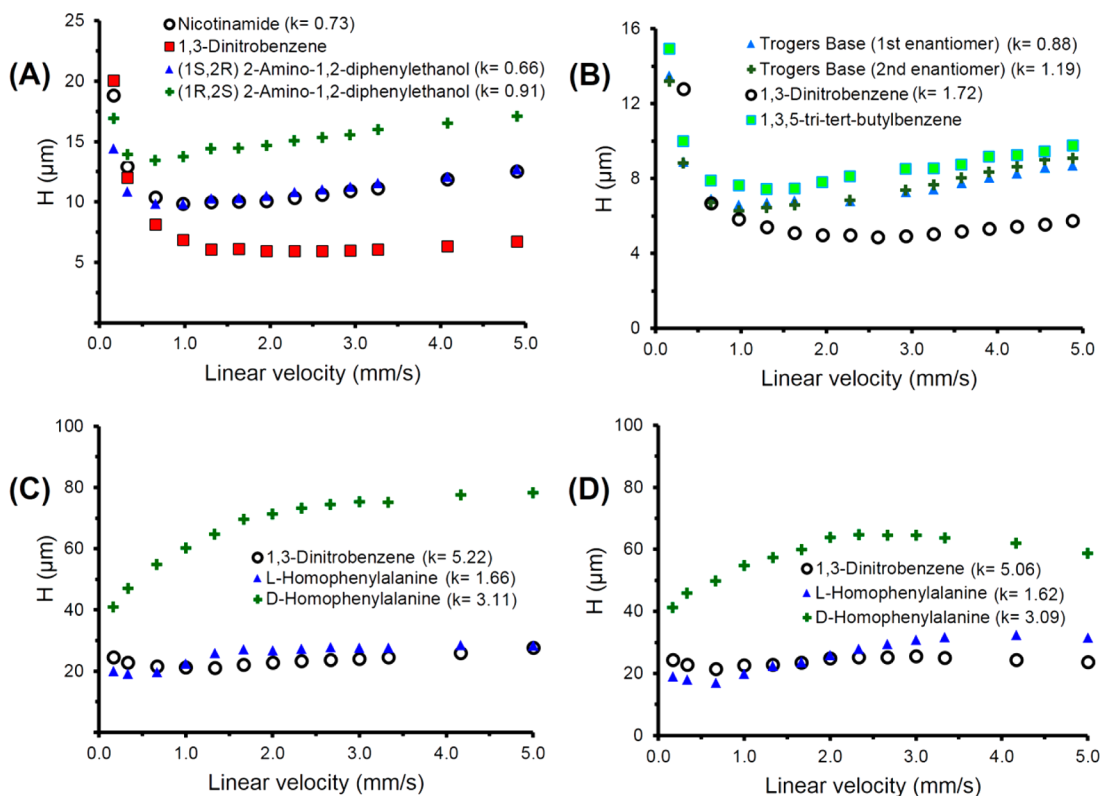


Figure 5. van Deemter plots for chiral and achiral analytes in polar organic mode, normal phase, and reversed phase on 2.7 μm SPP CSPs. (A) CF6-P SPP (10 cm × 0.46 cm i.d.), MP = 80:20:0.3:0.2 acetonitrile–methanol–TFA–TEA, $T_{\text{col}} = 25$ °C (thermostated). (B) CF7-DMP SPP (10 cm × 0.46 cm), MP = 90:10 heptane–ethanol, $T_{\text{col}} = 25$ °C (thermostated). (C) Teicoplanin bonded SPP (5 cm × 0.46 cm), MP = 90:10 water–methanol, $T_{\text{col}} = 25$ °C (thermostated). (D) $T_{\text{col}} = 22$ °C (not thermostated), other conditions were identical to part C. See the Supporting Information for temperature effects on selectivities. The k values reported are for a flow rate of 1 mL/min.

observed efficiencies in such van Deemter curves. Indeed, the highest efficiency column (CF7-DMP with a reduced plate height ($h = 1.6$)) was chosen for this example in an ultrafast format. Clearly under these conditions, one must be aware at all times of extra column effects and how they can generate apparent anomalous behaviors.⁵⁶

Figure 5C,D is for the same reversed phase enantiomeric separation and the same retained achiral analyte (1,3-dinitrobenzene). The only difference in these two series of experiments was that the column in Figure 5C was in a thermostated, temperature controlled, “still air device” set at 25 °C, while for Figure 5D the column was in ambient conditions (22 °C). It is well-known that teicoplanin chiral selectors strongly and selectively bind D-amino acid enantiomers and that this leads to greater resistance to mass transfer and broader peaks. This is confirmed by the upper plots for the more retained D-homophenylalanine in Figure 5C,D. Indeed no H minima vs linear velocity can be identified from these plots and the efficiencies are lower than those in the other mobile phase modes. It should be noted that such efficiencies can be greatly improved by judicious use of specific additives, but that is not the subject of this work. As in the polar organic mode, the curves for the first eluted (least retained) enantiomer and the achiral retained analyte (1,3-dinitrobenzene) are quite similar to one another and both show minima in the 0.5–1 mm/s region.

Perhaps the most striking aspect of these plots is the trend shown in Figure 5D. At linear velocities higher than ~2.5 mm/s, the efficiencies of both enantiomers and 1,3-dinitrobenzene begin to improve significantly. This effect is most pronounced

for the more retained D-homophenylalanine. It is well documented that two types of temperature gradients develop (axial and radial) when there is significant frictional heating.^{57,59,61,65} Eluents with the heat capacity and density of mobile phases used in Figure 5 (acetonitrile, heptane, and water) and operating pressures above 300 bar can easily generate axial temperature differentials of 10 °C.⁶¹ In fact, when the flow averaged temperature was measured at the column outlet at various linear velocities in three different modes, the axial temperature differences ranged from 11 to 16 °C (see the Supporting Information Tables S3–S5). This axial variation in fast separations does not contribute to an increase in peak width. On the other hand, the peak efficiency is significantly affected by radial temperature gradients which change local viscosities, velocity profiles, and diffusion coefficients of analytes.^{61,65} A first order “approximation” of the maximum radial temperature difference ΔT_{R} which can develop between the column center and the column wall is given by

$$\Delta T_{\text{R}} = \frac{u \left(\frac{dP}{dz} \right) R^2}{4\lambda_{\text{rad}}} \quad (2)$$

where u is the superficial flow velocity in m/s (obtained by dividing the volumetric flow rate by the total cross sectional area of the column), dP/dz the change in pressure in the direction of the column axis (z) per unit length in N/m³, R the column radius in m, and λ_{rad} is the approximate thermal conductivity of the mobile phase in the radial direction in W/m °C.⁶⁵

For example, in the normal phase mode (Figure 5B), the thermal conductivity of the heptane–ethanol mixture is approximately 0.13 W/m°C.⁶⁶ At low linear velocities, (1.67 mm/s or 1 mL/min, $\Delta P = 80$ bar), the magnitude of the maximum radial temperature difference is 1 °C; however, as the linear velocity is increased to 5 mm/s (3 mL/min), the pressure drop is significant (250 bar), and the calculated maximal radial temperature gradient is 8 °C. Note that eq 1 is generally used for first order approximations, it has been shown that the calculated radial temperature gradients can overestimate the observed radial gradients because it ignores the compressibility of the eluent. Consequently the actual energy generated in the column is reduced by a factor of 2/3.⁵⁹ On the other hand, as in Figure 5D, when a water-rich mobile phase is in use (thermal conductivity of 0.55 W/m°C), a linear velocity of 1.67 mm/s (1 mL/min) generated a back pressure of 112 bar due to higher viscosity. The calculated value of ΔT_R is only 1 °C, and at higher linear velocities, e.g., 5 mm/s (3 mL/min), a radial temperature difference of only 4 °C is developed. Also note that the axial temperature difference in Figure 5B,D was similar (~12 °C). However, the data used in Figure 5B was from a thermostated column (walls ~25 °C) while Figure 5D was not thermostated. Though, since heptane (Figure 5B) is far more compressible than water (Figure 5D), the energy produced is reduced by 2/3. However, it is clear from Figure 5D, that there are other factors, as in some chiral separations when resistance to mass transfer effects are more pronounced. In these interesting cases, such as a high thermal conductivity water rich mobile phase, the gain in efficiency from an improvement in mass transfer at higher axial temperature gradients is enough to visibly counter any smaller losses in efficiency due to radial temperature gradients and eddy dispersion. This possibility was noted early on by Halász⁶¹ and is apparent in Figure 5D. See the Supporting Information for detailed temperature measurements and calculations.

CONCLUSIONS

The results of this study, indicate that (1) SPPs are advantageous for ultrafast and high efficiency chiral separations, (2) enantiomeric separations on the order of few seconds are now feasible in all mobile phases with bonded brush type CSPs, (3) kinetic behaviors can sometimes be used to shed light on chiral recognition mechanisms, (4) CSPs can show quite different kinetic profiles from each other and from achiral systems, (5) ultrafast chiral separations require optimized detection and minimization of extra column effects, (6) frictional heating effects must be accounted for in ultrafast separations as they can manifest themselves in disparate ways and to different degrees for various CSPs and mobile phase modes, (7) efficiencies and separation speeds for chiral analytes can now exceed those in capillary electrophoresis. Also it is feasible to expect that (8) SPPs may be advantageous for preparative separations when their high efficiencies, faster analyses times, and reduced solvent consumption compensate for lower chiral selector loading, (9) ultrafast SPP-CSPs may be attractive as the second dimension in 2D-LC because of their greater selectivity and orthogonality to conventional achiral stationary phases, and (10) real-time monitoring of product formation in asymmetric synthesis is possible with ultrafast chiral separations.

ASSOCIATED CONTENT

Supporting Information

Peak parameter calculations, surface coverage of chiral selectors on silica, column permeability calculations, determination of extra-column contributions, and frictional heating measurements data. The Supporting Information is available free of charge on the ACS Publications website at DOI: 10.1021/acs.analchem.5b00715.

AUTHOR INFORMATION

Corresponding Author

*Phone: (817) 272-0632. Fax (817)-272-0619. E-mail: sec4dwa@uta.edu.

Notes

The authors declare no competing financial interest.

ACKNOWLEDGMENTS

The authors would like to acknowledge Agilent Technologies for providing the superficially porous particles. We also acknowledge the support of AZYP, LLC, Arlington, Texas.

REFERENCES

- (1) Davankov, V. A.; Rogozhin, S. V. *J. Chromatogr. A* **1971**, *60*, 280–283.
- (2) Mikes, F. E.; Boshart, G. *J. Chromatogr. A* **1978**, *149*, 455–464.
- (3) Pirkle, W. H.; Finn, J. M. *J. Org. Chem.* **1981**, *46*, 2935–2938.
- (4) Okamoto, Y.; Honda, S.; Okamoto, I.; Yuki, H.; Murata, S.; Noyori, R.; Takaya, H. *J. Am. Chem. Soc.* **1981**, *103*, 6971–6973.
- (5) Allenmark, S.; Bomgren, B.; Borén, H. *J. Chromatogr. A* **1983**, *264*, 63–68.
- (6) Armstrong, D. W.; Ward, T. J.; Armstrong, R. D.; Beesley, T. E. *Science* **1986**, *232*, 1132–1135.
- (7) Okamoto, Y.; Kawashima, M.; Yamamoto, K.; Hatada, K. *Chem. Lett.* **1984**, 739–742.
- (8) Armstrong, D. W.; DeMond, W. *J. Chromatogr. Sci.* **1984**, *22*, 411–415.
- (9) Okamoto, Y.; Aburatani, R.; Fukumoto, T.; Hatada, K. *Chem. Lett.* **1987**, 1857–1860.
- (10) Stalcup, A. M.; Chang, S. C.; Armstrong, D. W.; Pitha, J. *J. Chromatogr. A* **1990**, *513*, 181–194.
- (11) Armstrong, D. W.; Stalcup, A. M.; Hilton, M. L.; Duncan, J. D.; Faulkner, J. R., Jr.; Chang, S. C. *Anal. Chem.* **1990**, *62*, 1610–1615.
- (12) Pirkle, W. H.; Welch, C. J.; Lamm, B. *J. Org. Chem.* **1992**, *57*, 3854–3860.
- (13) Armstrong, D. W.; Tang, Y.; Chen, S.; Zhou, Y.; Bagwill, C.; Chen, J.-R. *Anal. Chem.* **1994**, *66*, 1473–1484.
- (14) Laemmerhofer, M.; Lindner, W. *J. Chromatogr. A* **1996**, *741*, 33–48.
- (15) Maier, N. M.; Nicoletti, L.; Laemmerhofer, M.; Lindner, W. *Chirality* **1999**, *11*, 522–528.
- (16) Berthod, A.; Chen, X. H.; Kullman, J. P.; Armstrong, D. W.; Gasparrini, F.; D'Acquarica, I.; Villani, C.; Carotti, A. *Anal. Chem.* **2000**, *72*, 1767–1780.
- (17) Gasparrini, F.; Misiti, D.; Rompietti, R.; Villani, C. *J. Chromatogr. A* **2005**, *1064*, 25–38.
- (18) Sun, P.; Wang, C. L.; Breitbach, Z. S.; Zhang, Y.; Armstrong, D. W. *Anal. Chem.* **2009**, *81*, 10215–10226.
- (19) Sun, P.; Armstrong, D. W. *J. Chromatogr. A* **2010**, *1217*, 4904–4918.
- (20) Han, X.; He, L.; Zhong, Q.; Beesley, T. E.; Armstrong, D. W. *Chromatographia* **2006**, *63*, 13–23.
- (21) Péter, A.; Török, G.; Armstrong, D. W.; Tóth, G.; Tourwé, D. *J. Chromatogr. A* **1998**, *828*, 177–190.
- (22) Davankov, V. A. *Chirality* **1997**, *9*, 99–102.
- (23) Gasparrini, F.; Misiti, D.; Villani, C. *Chirality* **1992**, *4*, 447–458.

- (24) Oberleitner, W. R.; Maier, N. M.; Lindner, W. *J. Chromatogr. A* **2002**, *960*, 97–108.
- (25) Sajonz, P.; Schafer, W.; Gong, X.; Shultz, S.; Rosner, T.; Welch, C. J. *J. Chromatogr. A* **2007**, *1145*, 149–154.
- (26) Hamman, C.; Wong, M.; Aliagas, I.; Ortwine, D. F.; Pease, J.; Schmidt, D. E., Jr.; Victorino, J. *J. Chromatogr. A* **2013**, *1305*, 310–319.
- (27) Ai, F.; Li, L.; Ng, S.-C.; Tan, T. T. Y. *J. Chromatogr. A* **2010**, *1217*, 7502–7506.
- (28) Cancelliere, G.; Ciogli, A.; D'Acquarica, I.; Gasparrini, F.; Kocergin, J.; Misiti, D.; Pierini, M.; Ritchie, H.; Simone, P.; Villani, C. *J. Chromatogr. A* **2010**, *1217*, 990–999.
- (29) Kotoni, D.; Ciogli, A.; Molinaro, C.; D'Acquarica, I.; Kocergin, J.; Szczerba, T.; Ritchie, H.; Villani, C.; Gasparrini, F. *Anal. Chem.* **2012**, *84*, 6805–6813.
- (30) Cavazzini, A.; Marchetti, N.; Guzzinati, R.; Pierini, M.; Ciogli, A.; Kotoni, D.; D'Acquarica, I.; Villani, C.; Gasparrini, F. *TrAC, Trends Anal. Chem.* **2014**, *63*, 95–103.
- (31) Gritti, F.; Guiochon, G. *LC–GC N. Am.* **2012**, 586–597.
- (32) Omamogho, J. O.; Nesterenko, E.; Connolly, D.; Glennon, J. *LC–GC N. Am.* **2012**, 63–69.
- (33) DeStefano, J. J.; Langlois, T. J.; Kirkland, J. J. *J. Chromatogr. Sci.* **2008**, *46*, 254–260.
- (34) Gritti, F. *LC–GC N. Am.* **2014**, 928–940.
- (35) Broeckhoven, K.; Cabooter, D.; Desmet, G. *J. Pharm. Anal.* **2013**, *3*, 313–323.
- (36) Bruns, S.; Stoeckel, D.; Smarsly, B. M.; Tallarek, U. *J. Chromatogr. A* **2012**, *1268*, 53–63.
- (37) Gritti, F.; Farkas, T.; Heng, J.; Guiochon, G. *J. Chromatogr. A* **2011**, *1218*, 8209–8221.
- (38) Dolzan, M. D.; Spudeit, D. A.; Breitbach, Z. S.; Barber, W. E.; Micke, G. A.; Armstrong, D. W. *J. Chromatogr. A* **2014**, *1365*, 124–130.
- (39) Spudeit, D. A.; Dolzan, M. D.; Breitbach, Z. S.; Barber, W. E.; Micke, G. A.; Armstrong, D. W. *J. Chromatogr. A* **2014**, *1363*, 89–95.
- (40) Fanali, S.; D'Orazio, G.; Farkas, T.; Chankvetadze, B. *J. Chromatogr. A* **2012**, *1269*, 136–142.
- (41) Lomsadze, K.; Jibuti, G.; Farkas, T.; Chankvetadze, B. *J. Chromatogr. A* **2012**, *1234*, 50–55.
- (42) Gritti, F.; Guiochon, G. *J. Chromatogr. A* **2014**, *1348*, 87–96.
- (43) Weatherly, C. A.; Na, Y.-C.; Nanayakkara, Y. S.; Woods, R. M.; Sharma, A.; Lacour, J.; Armstrong, D. W. *J. Chromatogr. B* **2014**, *955*–956, 72–80.
- (44) Armstrong, D. W.; Li, W.; Chang, C. D.; Pitha, J. *Anal. Chem.* **1990**, *62*, 914–923.
- (45) Jiang, C. X.; Tong, M. Y.; Breitbach, Z. S.; Armstrong, D. W. *Electrophoresis* **2009**, *30*, 3897–3909.
- (46) Zhang, Y.; Breitbach, Z. S.; Wang, C. L.; Armstrong, D. W. *Analyst* **2010**, *135*, 1076–1083.
- (47) Perera, S.; Na, Y.-C.; Doundoulakis, T.; Ngo, V. J.; Feng, Q.; Breitbach, Z. S.; Lovely, C. J.; Armstrong, D. W. *Chirality* **2013**, *25*, 133–140.
- (48) Padivitage, N. L. T.; Dodbiba, E.; Breitbach, Z. S.; Armstrong, D. W. *Drug Test. Anal.* **2014**, *6*, 542–551.
- (49) Woods, R. M.; Patel, D. C.; Lim, Y.; Breitbach, Z. S.; Gao, H. Y.; Keene, C.; Li, G. Q.; Kurti, L.; Armstrong, D. W. *J. Chromatogr. A* **2014**, *1357*, 172–181.
- (50) Woods, R. M.; Breitbach, Z. S.; Armstrong, D. W. *LC–GC N. Am.* **2014**, *32*, 742–751.
- (51) Fekete, S.; Kohler, I.; Rudaz, S.; Guillarme, D. *J. Pharm. Biomed. Anal.* **2014**, *87*, 105–119.
- (52) Wang, X.; Carr, P. W.; Stoll, D. R. *LC–GC N. Am.* **2010**, *28*, 932–942.
- (53) Elgass, H.; Engelhardt, H.; Halász, I. *Fresenius' Z. Anal. Chem.* **1979**, *294*, 97–106.
- (54) Guiochon, G.; Sepaniak, M. J. *Anal. Chem.* **1991**, *63*, 73–73.
- (55) Ma, Y.; Chassy, A. W.; Miyazaki, S.; Motokawa, M.; Morisato, K.; Uzu, H.; Ohira, M.; Furuno, M.; Nakanishi, K.; Minakuchi, H.; Mriziq, K.; Farkas, T.; Fiehn, O.; Tanaka, N. *J. Chromatogr. A* **2015**, *1383*, 47–57.
- (56) Usher, K. M.; Simmons, C. R.; Dorsey, J. G. *J. Chromatogr. A* **2008**, *1200*, 122–128.
- (57) de Villiers, A.; Lauer, H.; Szucs, R.; Goodall, S.; Sandra, P. *J. Chromatogr. A* **2006**, *1113*, 84–91.
- (58) Fountain, K. J.; Neue, U. D.; Grumbach, E. S.; Diehl, D. M. *J. Chromatogr. A* **2009**, *1216*, 5979–5988.
- (59) Gritti, F.; Guiochon, G. *Anal. Chem.* **2008**, *80*, 5009–5020.
- (60) Gritti, F.; Martin, M.; Guiochon, G. *Anal. Chem.* **2009**, *81*, 3365–3384.
- (61) Halász, I.; Endeke, R.; Asshauer, J. *J. Chromatogr. A* **1975**, *112*, 37–60.
- (62) Giddings, J. C. *Dynamics of Chromatography: Principles and Theory*, 1st ed.; CRC Press: Boca Raton, FL, 2002.
- (63) Boehm, R. E.; Martire, D. E.; Armstrong, D. W. *Anal. Chem.* **1988**, *60*, 522–528.
- (64) Gritti, F.; Guiochon, G. *J. Chromatogr. A* **2010**, *1217*, 6350–6365.
- (65) Poppe, H.; Kraak, J. C.; Huber, J. F. K.; van den Berg, J. H. M. *Chromatographia* **1981**, *14*, 515–523.
- (66) Qun-Fang, L.; Rui-Sen, L.; Dan-Yan, N.; Yu-Chun, H. *J. Chem. Eng. Data* **1997**, *42*, 971–974.